Phys Chem Minerals (2006) 33:629-637
DOI 10.1007/s00269-006-0111-0

ORIGINAL PAPER

P–V Equations of State and the relative stabilities of serpentine varieties

N. Hilairet · I. Daniel · B. Reynard

Received: 6 April 2006 / Accepted: 24 August 2006 / Published online: 12 October 2006

Abstract Serpentines are hydrous phyllosilicates which form by hydration of Mg–Fe minerals. The reasons for the occurrence of the structural varieties lizardite and chrysotile, with respect to the variety antigorite, stable at high pressure, are not yet fully elucidated, and their relative stability fields are not quantitatively defined. In order to increase the database of thermodynamic properties of serpentines, the *P–V* Equations of State (EoS) of lizardite and chrysotile were determined at ambient temperature up to 10 GPa, by in situ synchrotron X-ray diffraction in a diamond-anvil cell. Neither amorphization nor hysteresis was observed during compression and decompression, and no phase transition was resolved in lizardite. In chrysotile, a reversible change in compression mechanism, possibly due to an unresolved phase transition, occurs above 5 GPa. Both varieties exhibit strong anisotropic compression, with the *c* axis three times more compressible than the others. Fits to ambient temperature Birch–Murnaghan EoS gave for lizardite V_0=180.92(3) Å^3, K_0 = 71.0(19) GPa and K'_0=3.2(6), and for chrysotile up to 5 GPa, V_0 = 730.57(31) Å^3 and K_0 = 62.8(24) GPa (K'_0 fixed to 4). Compared to the structural variety antigorite is stable at high pressure (HP) (Hilairet et al. 2006), the *c* axis is more compressible in these varieties, whereas the *a* and *b* axes are less compressible. These differences are attributed to the less anisotropic distribution of stiff covalent bonds in the corrugated structure of antigorite. The three varieties have almost identical bulk compressibility curves. Thus the compressibility has negligible influence on the relative stability fields of the serpentine varieties. They are dominated by first-order thermodynamic properties, which stabilizes antigorite at high temperature with respect to lizardite, and by out-of-equilibrium phenomena for metastable chrysotile (Evans 2004).

Keywords Equation of state · Serpentines · XRD · Diamond anvil cell

N. Hilairet (✉) · I. Daniel · B. Reynard
Laboratoire des Sciences de la Terre,
UMR CNRS 5570, Ecole Normale Superieure de Lyon,
Université Claude Bernard Lyon 1, 46 allée d'Italie,
69364 Lyon Cedex 07, France
e-mail: Nadege.Hilairet@ens-lyon.fr

Introduction

Serpentines result from hydrothermal alteration of ultramafic rocks; they are among the major hydrous phases in oceanic lithosphere, and play a key role in the water cycle and in the subsequent element recycling processes. Indeed, serpentines are readily formed by hydration at mid oceanic ridges through hydrothermal alteration, and more slowly as the seafloor ages. There is also increasing speculation that, as the plate bends during subduction, its cold lithospheric mantle may become even more serpentinized (Ranero et al. 2003). While subduction proceeds, the downgoing oceanic lithosphere dehydrates at almost any depth to ca. 150–200 km (Schmidt and Poli 1998). Among hydrous minerals involved in the deep transport of water, serpentines may play a crucial role since the high-pressure form is stable to ca. 200 km depths, containing as much as 13 wt% (Ulmer and Trommsdorff 1995). Moreover, above the dehydrating slab, it is established that ascending hydrous fluids, released by metamorphic dehydration reactions, trigger partial melting in the

source region of arc magmas. These fluids may also induce significant serpentinization of the overlying peridotitic mantle wedge. Such serpentinites have been recognized in paleo-subduction zones (Guillot et al. 2001), and might actually be responsible for the exhumation of high-pressure to ultra-high-pressure rocks (Schwartz et al. 2001). Thus serpentines are formed in various geological settings, under different thermodynamic conditions, and occur as different structural varieties. The relative stabilities of the main varieties antigorite, lizardite, and chrysotile are only qualitatively understood. Determining the phase diagram of serpentine minerals in the MgO–FeO–SiO_2–H_2O (MSH) system requires accurately measuring their thermodynamic properties.

Serpentines are trioctahedral phyllosilicates, whose structure is based upon the stacking of a 1:1 layer composed of one octahedral and one tetrahedral sheet (Wicks and O'Hanley 1988). Different curvatures of this layer and various stacking schemes lead to three main structural varieties: lizardite has a planar structure, chrysotile has cylindrically rolled layers, and antigorite displays periodic reversals of the layer's polarity. For each of these, polytypism and polysomatism, and chemical variability, result in a great structural variability.

Antigorite is the predominant variety recovered in rocks showing high-pressure (HP) mineralogical assemblages (e.g. Mellini and Zanazzi 1987; Guillot et al. 2001), and has been shown experimentally to be the variety stable at HP–HT conditions (e.g. Evans 1976; Ulmer and Trommsdorff 1995; Wunder and Schreyer 1997). Its stability field has been recently re-evaluated with a new equation of state for antigorite (Hilairet et al. 2006).

The relative stability fields of lizardite and chrysotile are still poorly defined. Natural observations are very difficult because of the common intergrowth of several structural varieties. It has been proposed that chrysotile or lizardite appearance is related to crystallisation context and kinetics, rather than *P*–*T* conditions only (Evans 2004).

In order to progress in the determination of the *P*–*T* stability field and to better understand the relationship between crystallisation context and appearance of the different serpentine varieties, reliable Equations of State (EoS) for lizardite and chrysotile are necessary in addition to the one previously determined for antigorite (Hilairet et al. 2006). Hence, new measurements of the *P*–*V* EoS are presented here for lizardite and chrysotile, using in situ synchrotron X-ray diffraction (XRD) in a membrane diamond anvil cell (DAC), up to ~10 GPa at ambient temperature.

Experimental methods

Sample characterization

The samples used in this study are natural samples described in detail by Auzende et al. (2004). Briefly, the lizardite sample comes from Monte Fico (Elba Island), and has a structural formula $(Mg_{2.75}Al_{0.09}Fe_{0.16})_{\Sigma=3}(Si_{1.92}Al_{0.08})_{\Sigma=2}O_5(OH)_4$. The chemistry and the structure of this material have been studied in detail by Mellini and Viti (1994) and Fuchs et al. (1998). It contains only minor quantities of chrysotile (<5%) (Viti and Mellini 1997).

The antigorite sample Cu12 comes from the Escambray massif, located in the paleo-subduction zone of Central Cuba. Its structural formula is $(Mg_{2.62}Fe_{0.16}Al_{0.15})_{\Sigma=2.93}(Si_{1.96}Al_{0.04})_{\Sigma=2}O_5(OH)_{3.57}$. It is a one layer polytype with an average $m = 14$ superperiodicity, determined by HTREM (Auzende et al. 2002). The initial rock contains less than 5 wt% chrysotile, and exhibits small variations in the structural parameter *m*, both of which are common features of antigorite.

The chrysotile sample originates from the asbestos mines of Thetford (Quebec). It has been previously characterized by XRD (Lemaire et al. 1999) and corresponds to the monoclinic type (clinochrysotile).

High pressure and volume measurement techniques

The samples were ground to micron-sized grains (~2–5 μm) in an agate mortar. Samples were pressurized in a membrane-type diamond anvil-cell (Chervin et al. 1995). X-ray diffraction measurements were carried out with a monochromatic synchrotron beam (λ = 0.3738 Å for lizardite and chrysotile and 0.3706 Å for antigorite, respectively), at the ID30 beamline of the European Synchrotron Radiation Facility (Grenoble, France), during compression and decompression. Pressure was measured with the ruby fluorescence technique (Mao et al. 1986). The pressure transmitting medium was a 16:4:1 methanol–ethanol–water mixture, which ensures hydrostatic conditions up to the highest pressures reached here of 10 GPa. Diffraction patterns were collected with a MAR®345 detector. The characteristic exposure time for diffraction was 60 s. The sample to detector distance was calibrated against a Silicon standard. The Fit2D software (Hammersley et al. 1996) was used to apply tilt and distortion correction, and to integrate the 2D patterns.

Lattice parameters were refined in the procedure of Le Bail et al. (1988), with the GSAS package (Larson and Von Dreele 2004). In this procedure, initial

structure factors are calculated from assumed atomic positions, which were chosen from available structural refinements on natural serpentines. The structure factors are then adjusted by least-square methods during the refinement, and not extracted from assumed atomic positions, which therefore have little effect on the final results. For the refinement of lizardite cell parameters, we used the P31 m space group and atomic positions from Lizardite 1*T* MFN3–6, (Mellini and Viti 1994). For antigorite, we used the Pm space group, lattice cell parameters, and atomic positions from antigorite-1*T* $m = 17$ (Capitani and Mellini 2004), as no refinement for unit-cell atomic positions in the $m = 14$ polysome is available. Using the $m = 17$ cell parameters and structure instead of those for $m = 14$ has negligible effect on refined $m = 1$ volumes and on a/a_0 and V/V_0 variation. However the resulting V, the a lattice parameter, and the diffraction peak indexes obtained are affected by a factor 17/14 compared to the real ones, and must not be taken as absolute values. For chrysotile, we used the C2/m space group with starting cell parameters of clinochrysotile at ambient pressure, and lizardite 1*T* atomic positions (Mellini and Viti 1994), as no atomic positions refinement was available for clinochrysotile.

The (P, V) data were adjusted to a second- and third-order Birch–Murnaghan EoS (B–M EoS) using the EoSfit5.2 software (Angel 2001). Data points were weighted by an estimated 3% P uncertainty and by estimated standard deviation on V [esd(V), 1σ] from diffraction peak fitting (Table 1). Linear compressibilities were also fitted with EoSFit5.2.

Results

Figure 1a, b displays selected diffraction patterns of lizardite and antigorite, at 3.5 and 4.9 GPa, respectively. Although there is an excellent agreement in the position of the diffraction lines between the data and the calculated spectra, up to the highest values of two-theta, some small intensity mismatch is always observed in the residuals. This is partly due to the refinement procedure used which aims mainly at matching peak positions. This might also be due to preferred orientations, which cannot be avoided in minerals with a planar or fibrous habit. However, the intensity mismatch is small, and reliable unit-cell parameters could be extracted without refining the texture of the samples.

Within the investigated pressure range, none of the serpentine varieties displays any sign of amorphization, as illustrated by the series of diffraction patterns of chrysotile (Fig. 1c). The diffraction pattern of each variety could be indexed in the same space group, up to the maximum pressure.

The lattice parameters of lizardite and chrysotile (Table 1) are reported as a function of pressure in Fig. 2. The results for antigorite (Hilairet et al. 2006) have been added for the sake of completeness and for discussion. The data obtained along the decompression path do not display any hysteresis, and thus confirms that the hydrostatic compression of antigorite, lizardite, and chrysotile to 10 GPa is fully reversible (Auzende et al. 2004; Reynard and Wunder 2006). The parameters resulting from the EoS fits, and calculated axis compressibilities at P_0 are listed in Table 2. In the following, the subscript 0 on V and K stands for the standard condition $P = 10^5$ Pa, and $T = 298$ K.

Compressibility curves for the unit-cell parameters are displayed in Fig. 2. As expected from the behaviour of other known layer silicates, all serpentine varieties exhibit pronounced anisotropic compression. They are much more compressible along the [001] direction, which is normal to the TO layers, than along the a and b axes, oriented within the layers. Therefore the TO interlayer thickness decreases rapidly as a function of pressure. At 10 GPa, it is already reduced by 5–6%.

The anisotropy in compression is more pronounced in lizardite and chrysotile than in antigorite. With respect to [100], the axial compression ratios are 3:1 in lizardite and chrysotile, whereas in antigorite, this ratio is only 2:1. The origin of such a large difference is twofold: the axial compressibility of the [001] axis in antigorite is slightly smaller than in lizardite and chrysotile, while that of the [100] and [010] axis in antigorite is significantly larger than in lizardite and chrysotile (Fig. 2).

Variations in the β angle with pressure for the antigorite and chrysotile varieties are also displayed in Fig. 2. The monoclinic distortion in antigorite slightly decreases as pressure increases. The changes in the distorsion angle are quite large in chrysotile, reversing sign at 5 GPa. At low pressure, the β angle decreases at –0.27° GPa^{-1} from 93.5° to 92.25° at 5 GPa. At higher pressure, it increases rapidly at 0.43° GPa^{-1}, and reaches 94° at ca. 10 GPa. This could be an artefact from the refinement procedure, which is not very stable in the case of many small peaks overlapping, and may give different indexes to the same peak from one pattern to another. If not an artefact, this important change in compression mechanism around 5 GPa, may be attributed to a phase transition, although unresolved in the diffraction pattern.

Table 1 Unit-cell parameters of lizardite, antigorite (from Hilairet et al. 2006), and chrysotile, during compression and decompression, obtained from XRD pattern refinements with the GSAS package

Pressure (GPa) ± 3%		V (Å^3)	a (Å)	b (Å)	c (Å)	β (deg)
Lizardite						
0.0001	0.00003	180.909 (17)	5.3477 (2)	–	7.3045 (6)	–
0.41	0.01	179.972 (29)	5.3418 (3)	–	7.2829 (11)	–
0.64	0.02	179.508 (28)	5.3395 (3)	–	7.2704 (10)	–
0.97	0.03	178.132 (32)	5.3328 (2)	–	7.2326 (12)	–
1.50	0.04	177.030 (27)	5.3270 (2)	–	7.2036 (10)	–
2.01	0.06	176.296 (26)	5.3228 (2)	–	7.1850 (11)	–
2.80	0.08	174.453 (64)	5.3127 (3)	–	7.1372 (24)	–
3.54	0.11	172.920 (19)	5.3035 (2)	–	7.0990 (7)	–
4.67	0.14	170.776 (25)	5.2898 (2)	–	7.0473 (9)	–
5.34	0.16	169.317 (24)	5.2802 (2)	–	7.0125 (9)	–
6.36	0.19	167.376 (26)	5.2655 (2)	–	6.9707 (9)	–
7.79	0.23	164.464 (25)	5.2416 (2)	–	6.9121 (9)	–
8.26	0.25	163.514 (24)	5.2336 (2)	–	6.8932 (9)	–
9.57	0.29	161.443 (25)	5.2144 (2)	–	6.8560 (9)	–
10.40	0.31	160.581 (27)	5.2065 (2)	–	6.8403 (10)	–
9.64	0.29	161.379 (22)	5.2146 (2)	–	6.8529 (8)	–
9.04	0.27	162.149 (22)	5.2200 (2)	–	6.8668 (9)	–
8.07	0.24	163.961 (22)	5.2380 (2)	–	6.9006 (9)	–
6.81	0.20	166.684 (25)	5.2599 (2)	–	6.9567 (10)	–
3.39	0.10	173.252 (24)	5.3067 (2)	–	7.1040 (9)	–
0.92	0.03	178.560 (27)	5.3380 (2)	–	7.2359 (10)	–
Antigorite[a]						
0.0001	0.00003	2927.200 (249)	43.5590 (15)	9.2597 (3)	7.2590 (6)	91.264 (5)
0.25	0.01	2912.922 (266)	43.5195 (21)	9.2521 (5)	7.2362 (5)	91.264 (6)
0.68	0.02	2897.092 (217)	43.4692 (17)	9.2467 (3)	7.2094 (4)	91.257 (6)
1.95	0.06	2842.292 (237)	43.2608 (24)	9.2126 (6)	7.1332 (5)	91.183 (7)
2.86	0.09	2814.499 (246)	43.1591 (28)	9.1890 (5)	7.0980 (5)	91.090 (7)
3.81	0.11	2783.744 (269)	43.0156 (26)	9.1597 (4)	7.0665 (6)	91.122 (9)
4.94	0.15	2752.398 (213)	42.8450 (22)	9.1279 (3)	7.0389 (4)	90.992 (6)
5.87	0.18	2718.505 (034)	42.7178 (33)	9.1023 (4)	6.9922 (7)	90.803 (9)
7.03	0.21	2689.081 (352)	42.5941 (04)	9.0727 (4)	6.9592 (7)	90.800 (10)
8.05	0.24	2650.289 (182)	42.4336 (25)	9.0252 (6)	6.9213 (3)	90.979 (10)
8.49	0.25	2645.977 (286)	42.3631 (26)	9.0280 (4)	6.9191 (5)	90.809 (7)
9.00	0.27	2628.157 (231)	42.2930 (27)	9.0121 (5)	6.8962 (4)	90.886 (10)
9.45	0.28	2623.060 (244)	42.2413 (18)	9.0061 (4)	6.8958 (5)	90.850 (6)
9.98	0.30	2610.730 (272)	42.2876 (23)	8.9783 (5)	6.8772 (6)	90.943 (5)
7.82	0.23	2661.707 (264)	42.4364 (21)	9.0436 (5)	6.9363 (5)	90.863 (7)
4.98	0.15	2755.339 (233)	42.8703 (16)	9.1376 (3)	7.0345 (5)	90.863 (6)
3.10	0.09	2810.150 (366)	43.1104 (23)	9.1833 (7)	7.0995 (7)	91.080 (9)
1.16	0.03	2873.300 (254)	43.4110 (16)	9.2252 (5)	7.1766 (5)	91.278 (6)
Chrysotile						
0.96	0.03	718.465 (253)	5.3700 (22)	9.1485 (24)	14.6456 (37)	93.078 (23)
1.24	0.04	716.297 (255)	5.3684 (22)	9.1449 (20)	14.6110 (37)	93.043 (23)
2.92	0.09	700.157 (224)	5.3452 (13)	9.0997 (15)	14.4085 (32)	92.520 (21)
3.89	0.12	693.110 (207)	5.3334 (12)	9.0799 (14)	14.3249 (26)	92.375 (22)
5.13	0.15	686.563 (355)	5.3268 (18)	9.0613 (22)	14.2347 (44)	92.227 (35)
6.43	0.19	676.776 (183)	5.3048 (13)	9.0291 (20)	14.1445 (26)	92.624 (18)
7.98	0.24	664.839 (183)	5.2857 (9)	8.9838 (20)	14.0263 (19)	93.456 (13)
8.50	0.25	660.476 (174)	5.2730 (6)	8.9765 (19)	13.9900 (17)	93.519 (11)
9.07	0.27	655.724 (171)	5.2654 (7)	8.9539 (18)	13.9384 (19)	93.766 (14)
9.36	0.28	653.564 (161)	5.2657 (5)	8.9363 (19)	13.9216 (20)	93.918 (23)
3.67	0.11	695.163 (230)	5.3354 (14)	9.0909 (18)	14.3458 (31)	92.501 (22)
2.29	0.07	706.217 (233)	5.3532 (12)	9.1216 (16)	14.4794 (33)	92.744 (20)
0.0001	0.00003	730.684 (137)	5.3865 (7)	9.1754 (14)	14.8128 (23)	93.559 (14)

For antigorite, the reported cell parameters are calculated using the m = 17 polysome dimension, rather than m = 14. Uncertainty on pressure estimated to be 3%. Esd (1σ) given in brackets on the last decimals

[a] From Hilairet et al. (2006)

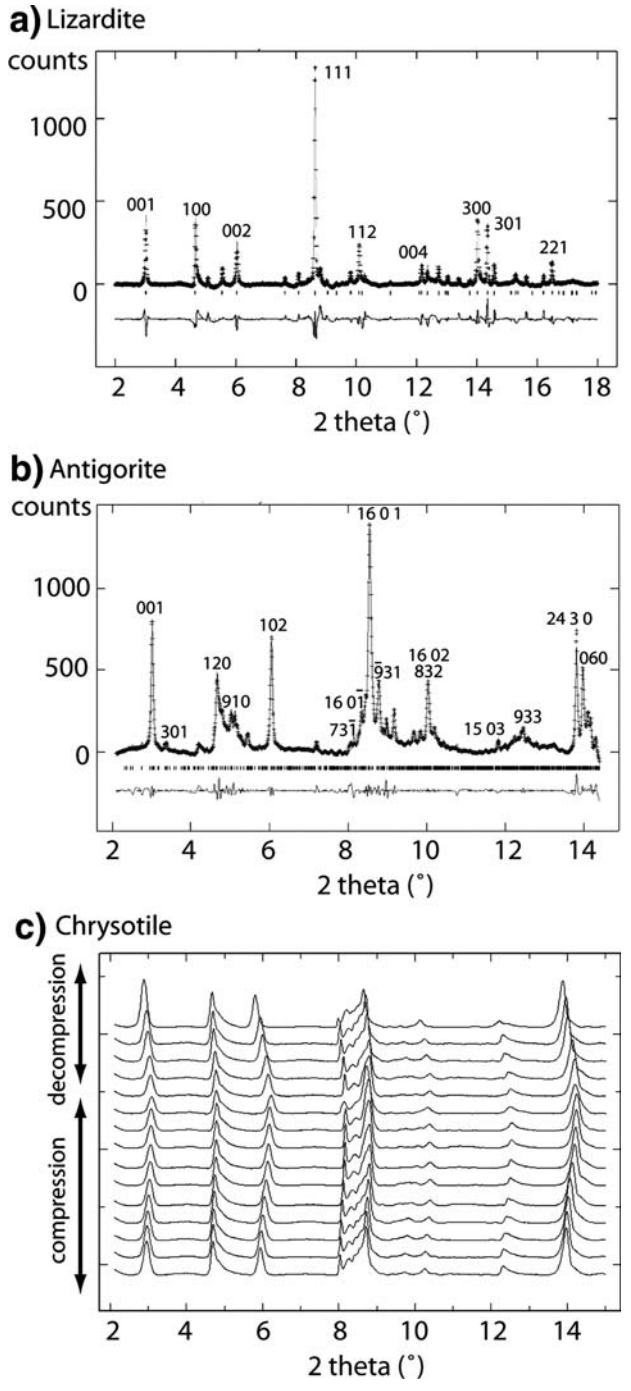

Fig. 1 XRD spectra for lizardite (**a**) and antigorite (**b**) at 3.5 and 4.9 GPa, respectively. *Crosses* represent the data, the *solid line* corresponds to the pattern calculated with the GSAS package. *Main peaks* are indexed. Antigorite results are from Hilairet et al. (2006); the peak indexes are the equivalent peaks for the $m = 17$ polysome rather than $m = 14$, as we used $m = 17$ for the refinement. *Residuals* are shown below the spectra; they are mostly due to intensity miscalculations. (**c**) Chrysotile XRD patterns during compression and decompression (from *bottom to top*). The peaks remain sharp during compression and decompression, showing that no amorphization occurred during the whole experiment

Variations of V/V_0 with pressure are plotted for lizardite and chrysotile along with the EoS fits in Fig. 3. Antigorite EoS is also shown for comparison (Hilairet et al. 2006). The compressibility curves for the structural varieties chrysotile and lizardite are very similar, and close to that of antigorite ($K_0 = 67.3(12)$ GPa with $K' = 4$; Hilairet et al. 2006). The P–V compression curve for lizardite agrees well with that proposed by Mellini and Zanazzi (1989), except for their last data point which lies significantly under our curve. For chrysotile, a break in the compression curve occurs between 4 and 5 GPa. Between 5 and 8 GPa, the unit-cell volume of chrysotile is slightly larger than expected from the compressibility at lower pressure. Non-hydrostatic effects cannot be advocated to account for this observation because we took care of dispersing as little powder as possible in the pressure medium, which is still liquid at these pressures. This break takes place in conjunction with the change in the pressure dependence of the beta angle, to which it is more likely to be related. Therefore, the adjustment of the P–V data for chrysotile to a Birch–Murnaghan EoS was performed for the whole dataset, as well as for a restricted dataset limited to 5 GPa.

Compression curves of lizardite and chrysotile were adjusted to second and third order Birch–Murnaghan EoS. A least-squares fit of the data yields the following room pressure parameters, also summarized in Table 2. For lizardite, $V_0 = 180.92(3)$ Å^3, $K_0 = 71.0(19)$ GPa and $K'_0 = 3.2(6)$, and $K_0 = 68.9(9)$ if K'_0 is set to 4. For antigorite, $V_0 = 2926.23(50)$ Å^3, $K_0 = 62.0$ (22) GPa and $K'_0 = 6.4(10)$, and $K_0 = 67.2(1)$ if K'_0 is set to 4. For chrysotile, $V_0 = 730.57(31)$ Å^3 and $K_0 = 62.8(24)$ GPa ($K'_0 = 4$) below 5 GPa, and $V_0 = 730.57(31)$ Å^3 and $K_0 = 66.5(15)$ GPa ($K'_0 = 4$) up to 9 GPa. Since the K'_0 value for the 3rd order EoS for chrysotile is unconstrained and unrealistically high; we favour values from the fit to the second order. Qualitatively, F–f plots (Angel 2001) confirm the slight differences between the parameters obtained from the fits, requiring a 3rd order EoS for lizardite, and a 2nd order EoS for chrysotile (below 5 GPa). They show that V_0 estimations are correct. Moreover, K_0 and K'_0 values estimated from the F–f plots are in good agreement with the results from the least-square fits.

Discussion

The similarity between the compression curves of the three investigated serpentine varieties confirms that they macroscopically compress in a similar way

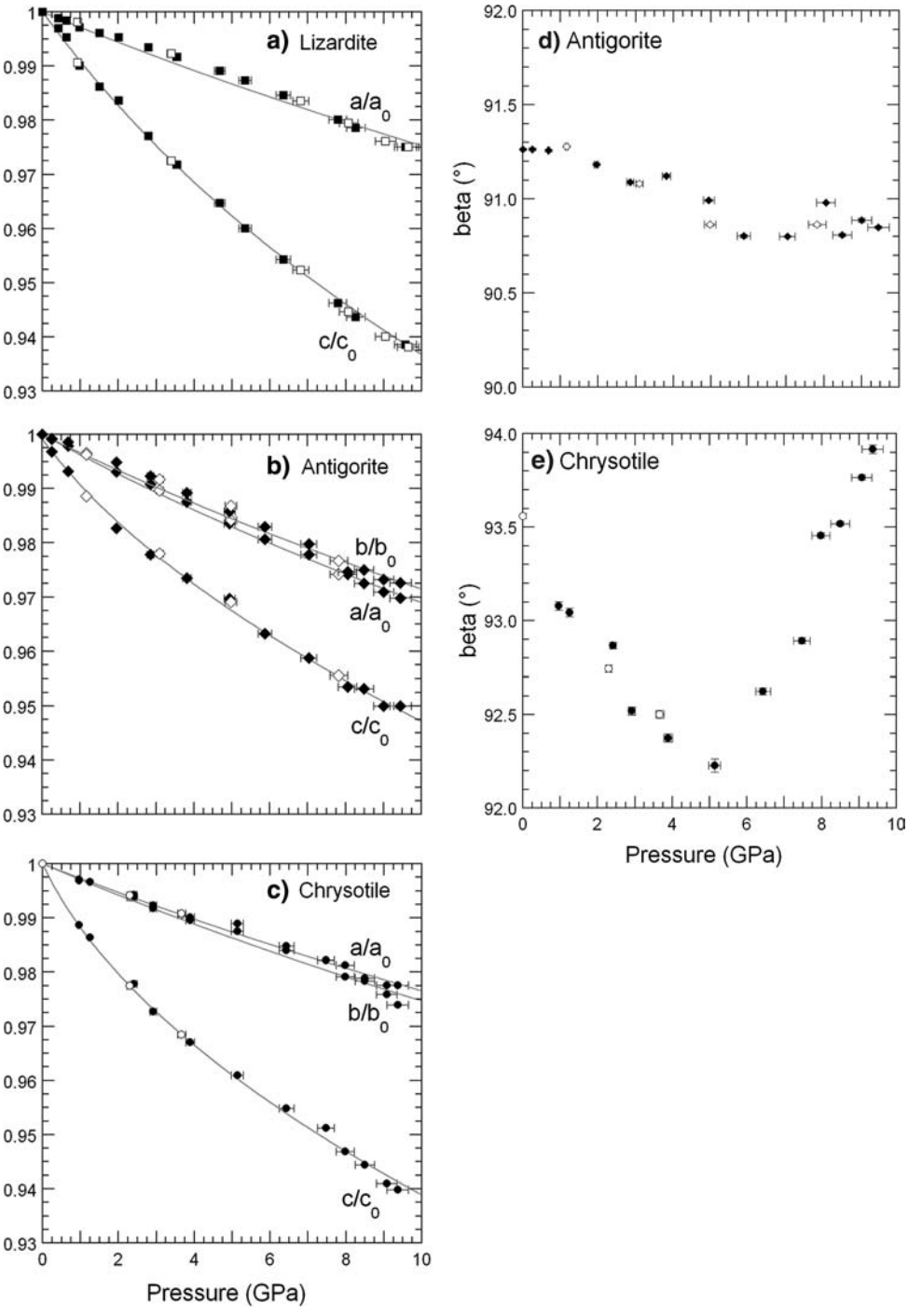

Fig. 2 Normalized lattice parameters variation against pressure for lizardite, antigorite, and chrysotile. *Filled and empty symbols* are for data collected during compression and decompression, respectively. The *lines* are only guidelines and do not represent EoS fits. Standard deviations (1σ) on lattice parameters are smaller than data points except when indicated, and *errors bars* on pressure correspond to a 3% uncertainty

(Auzende et al. 2004), despite important structural differences.

Standard state unit-cell parameters and volume obtained here are specific to these samples and integrated over the sample's structural variability. The bulk modulus might vary between different polysomes and polytypes, and also with the fiber radius in the case of chrysotile. However, as the compression curves are similar for three different structural varieties, it is unlikely that polytypism and polysomatism in serpentines lead to variations in bulk compressibility large enough to modify further stability field calculations. In a multiphase assemblage, the variation with pressure of the antigorite polysome, proposed by Wunder and Schreyer 1997, has therefore no effect on the bulk compressibility.

The compression curve of chrysotile is characterized by an abrupt change in β variation and a departure of V/V_0 from the curve defined by the data

Table 2 Thermodynamic parameters obtained from the fitting of second and third order Birch–Murnaghan EoS to compression data

	V_0 (Å^3)	K_0 (GPa)	K'_0
Lizardite	180.93 (3)	68.9 (9)	4[a]
	180.92 (3)	71.0 (19)	3.2 (6)
Chrysotile	730.57 (31)	62.8 (24)	4[a]
(below 5 GPa)	730.67 (23)	54.1 (45)	13.0 (50)
(to 9 GPa)	730.42 (29)	66.5 (15)	4[a]
	730.60 (23)	59.7 (25)	7.2 (12)
Antigorite	2926.23 (50)	67.3 (12)	4[a]
	2926.65 (47)	62.0 (22)	6.4 (10)
Linear compressibilities (GPa^{-1}) at P_0=10^{-4} GPa, $\beta_0 = l_0^{-1}(\partial l/\partial P)_{P=0}$			
	β_a	β_b	β_c
Lizardite	0.002735	–	0.009707
Chrysotile	0.002731	0.002774	0.011099
Antigorite	0.003693	0.003336	0.008266

Antigorite results are from Hilairet et al. (2006). Esd (1σ) given within brackets on the last decimals

[a] Fixed parameter

points below 5 GPa (Fig. 2b, e). At 8 GPa the volume variation of chrysotile lies again on the curve defined by the B–M EoS fit below 5 GPa, and a break may also be seen in β variation. These features might be explained by an artefact of the fitting procedure, or by two reversible changes in compression mechanisms around 5 and 8 GPa. Chrysotile unit cell contains two 1:1 layers, which can be stacked in different ways, giving different polytypes. Therefore the β angle in chrysotile depends on the stacking of the unit cells, i.e. the shift along the a axis from the first layer to the next unit-cell first layer. The observed variations of β (Fig. 2e) cover a range of values corresponding to the polytypes 1Mc2, 2Mc1, and 1Mc1 (Wicks and O'Hanley 1988). Despite the large and complicated variations of the β angle as a function of pressure, the layer thickness expressed as $c.\sin\beta$ displays a continuous and monotonous behaviour. Thus, if the observed scatter is not due to a fitting artefact, the transitions marked by the evolution of β and V/V_0 with pressure may indicate inter-layer re-arrangements, or may be due to unresolved reversible phase transitions.

The f–F plots (Angel 2001), and comparison of the K_0 and K' parameters of the Birch–Murnaghan EoS between serpentines (Table 2), show that only subtle distinctions can be made between the varieties investigated here. Antigorite is slightly more compressible than lizardite at ambient conditions, but less than chrysotile. Auzende et al. (2004) suggested that the greater mean pressure dependence of antigorite Raman stretching modes, when compared to the other structural varieties, might reflect a higher bulk compressibility of antigorite. This proposition is not supported by the present results.

The c axis compressibility varies significantly between antigorite and the two other varieties, while the pressure dependence of the Raman stretching frequencies of outer hydroxyl groups situated in the interlayer space are similar for all three varieties (Auzende et al. 2004). Therefore, the evolution of the stretching frequencies of the outer OH as a function of pressure and eventually the evolution of hydrogen bonding do not correlate with the decrease in the interlayer distance, or the compressibility of the c axis. We attribute the smaller compressibility of the c axis in antigorite than in lizardite and chrysotile to the presence of stiff ionic bonds in that direction at the layers reversal of the corrugated structure.

The bulk moduli K_0 of the three structural varieties are similar within experimental uncertainties. Thus compressibility has little effect on the relative stability of the different varieties, and cannot help resolving the problem of the stability fields of serpentine varieties. Currently, most of the thermodynamic calculations use Berman (1988) or Holland and Powell (1998) self-consistent databases, in which the same value of K_0 is used for antigorite and chrysotile. The assumption of a similar K_0 and $K'_0 = 4$ is justified by the present results. However, the higher values obtained here for K_0 show that calculations using these databases overestimate the stability fields of serpentines towards high pressures (Hilairet et al. 2006). In the system with lizardite/chysotile stoichiometry and under water saturation, lizardite and chrysotile are expected to transform to antigorite according to: 17 liz/chrys $\rightarrow$ atg + 3 br (1). With the available data, chrysotile with ideal $Mg_3Si_2O_5(OH)_4$ formula is always metastable with respect to antigorite-bearing assemblages, and its occurrence in low pressure low temperature hydrated

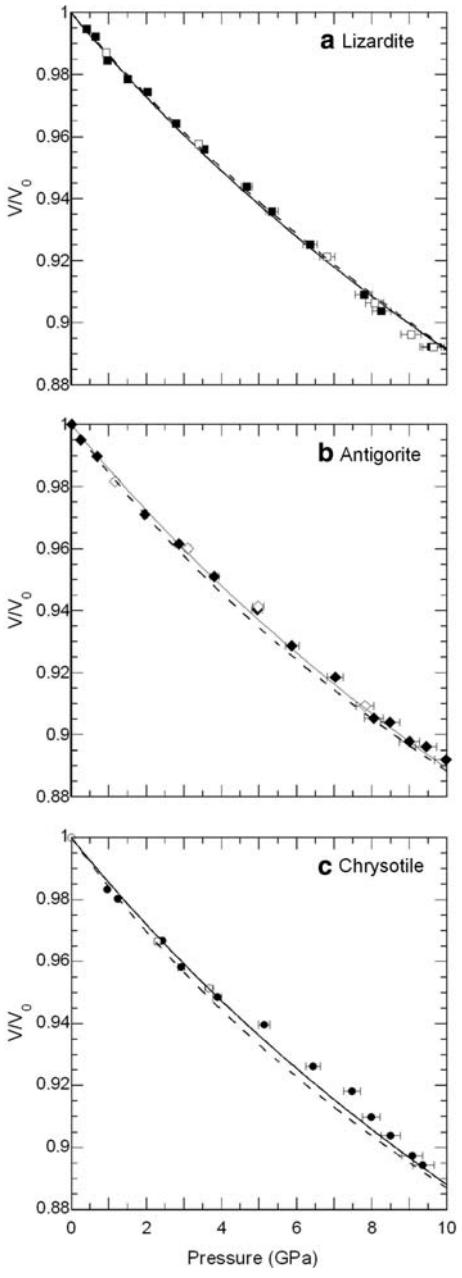

Fig. 3 Normalized compression curves at ambient temperature for lizardite, antigorite and chrysotile. *Filled and open symbols* represent data collected during compression and decompression, respectively. Standard deviation (1σ) on volume is smaller than data points, and *errors bars* on pressure correspond to a 3% uncertainty. Data are fitted with second (*full line*) and third (*dotted line*) order Birch–Murnaghan EoS. For Chrysotile, the curves correspond to the EoS derived from data below 5 GPa, only

ultramafic rocks or as a retrogressive product of antigorite and lizardite is likely due to out-of-equilibrium processes (Evans 2004). In the absence of phase equilibrium data and calorimetric measurements for lizardite, its stability field may be estimated by placing bounds on its free enthalpy of formation and its entropy. The volume change for reaction (1) involving chrysotile and lizardite can be estimated from recent X-ray determinations for close-to-end-member compositions (Capitani and Mellini 2004 for antigorite, Mellini and Viti 1994 for lizardite). The value is close to zero at every pressure using our compressibilites (–0.48 at ambient pressure to –0.98 J bar^{-1} at 6 GPa), indicating that the lizardite to antigorite-bearing assemblage reaction is pressure-independent if the entropy change is significant. Thus the phase diagram proposed by Evans (2004) can be extended to higher pressure if his assumptions on entropy changes are valid.

The determined compressibilities will provide additional constraints for improving ab initio and atomistic modelling of bonding in serpentines (Benco and Smrcok 1998, Balan et al. 2002). These calculations are at the moment the most efficient way to explore serpentines elastic properties, to obtain vibrational models for entropy calculations and determination of reaction free enthalpy changes. Such models or calorimetric measurements on lizardite are needed for calculations of stability fields, finally providing the best mineralogical properties required to understand geophysical data on oceanic floors, in subduction zones and major fault zones.

Acknowledgments We thank Wilson Crichton for assistance during the experiments; constructive reviews by M. Mellini and B. Evans were greatly appreciated and helped improve the manuscript. This work was financially supported by DyETI program of the French Institut National de Sciences de l'Univers.

References

Angel RJ (2001) Equations of State, in high-pressure, high-temperature crystal chemistry. In: Hazen RM, Downs RT (eds) Reviews in Mineralogy and Geochemistry, pp 35–60

Auzende A-L, Devouard B, Guillot S, Daniel I, Baronnet A, Lardeaux J-M (2002) Serpentinites from Central Cuba: petrology and HRTEM study. Eur J Mineral 14:905–914

Auzende A-L, Daniel I, Reynard B, Lemaire C, Guyot F (2004) High-pressure behavior of serpentine minerals: a Raman spectroscopic study. PhysChem Minerals 31:269–277

Balan E, Saitta AM, Mauri F, Lemaire C, Guyot F (2002) First-principles calculation of the infrared spectrum of lizardite. Am Mineral 87:1286–1290

Benco L, Smrcok L (1998) Hartree–Fock study of pressure-induced strengthening of hydrogen bonding in lizardite-1T. Eur J Mineral 10:483–490

Berman RG (1988) Internally-consistent thermodynamic data for minerals in the system Na_2O–K_2O–CaO–MgO–FeO–Fe_2O_3–Al_2O_3–SiO_2–TiO_2–H_2O–CO_2. J Petrol 29:445–522

Capitani G, Mellini M (2004) The modulated crystal structure of Antigorite: the m = 17 polysome. Am Mineral 89:147–158

Chervin JC, Canny B, Besson J-M, Pruzan P (1995) A diamond-anvil cell for IR microspectrometry. Rev Sci Instrum 66:2595–2598

Evans BW (1976) Stability of chrysotile and antigorite in the serpentinite multisystem. Schweiz Min Pet Mitt 56:79–93

Evans BW (2004) The serpentinite multisystem revisited: Chrysotile is metastable. Int Geol Rev 46:479–506

Fuchs Y, Linares J, Mellini M (1998) Mössbauer and infrared spectrometry of lizardite-1T from Monte-Fico Elba. Phys Chem Miner 26:111–115

Guillot S, Hattori K, de Sigoyer J, Nägler T, Auzende A-L (2001) Evidence of hydration of the mantle wedge and its role in the exhumation of eclogites. Earth Planet Sci Lett 193:115–127

Hammersley AP, Svensson SO, Hanfland M, Fitch AN, Häusermann D (1996) Two-dimensional detector software: from real detector to idealised image or two-theta scan. High Pressure Res 14:235–248

Hilairet N, Daniel I, Reynard B (2006) Equation of state of antigorite, stability field of serpentines, and seismicity in subduction zones. Geophys Res Lett 33:L02302, doi:10.1029/2005GL024728

Holland TJB, Powell R (1998) An internally consistent thermodynamic data set for phases of petrological interest. J Metam Geol 16:309–343

Larson AC, Von Dreele RB (2004) General Structure Analysis System (GSAS), Los Alamos National Laboratory

Le Bail A, Duroy H, Fourquet JL (1988) Ab-initio structure determination of $LiSbWO_6$ by X-ray powder diffraction. Mater Res Bull 23:447–452

Lemaire C, Guyot F, Reynard B (1999) Vibrational spectroscopy (IR and Raman) of OH groups in chrysotile, lizardite and antigorite, presented at European Union of Geosciences 10, Strasbourg pp 654

Mao HK, Xu J, Bell PM (1986) Calibration of the ruby pressure gauge to 800 kbar uner quasi-hydrostatic conditions. J Geophys Res 91:4763–4767

Mellini M, Viti C (1994) Crystal structure of Lizardite-1T from Elba, Italy. Am Mineral 79:1194–1198

Mellini M, Zanazzi PF (1987) Crystal structures of Lizardite-1T and Lizardite-2H1 from Coli, Italy. Am Mineral 72:943–948

Mellini M, Zanazzi PF (1989) Effects of pressure on the structure of Lizardite 1T. Eur J Mineral 1:13–19

Ranero CR, Phipps Morgan J, McIntosh K, Reichert C (2003) Bending-related faulting and mantle serpentinization at the Middle America trench. Nature 425:367

Reynard B, Wunder B (2006) High-pressure behavior of synthetic antigorite in the $MgO–SiO_2–H_2O$ system from Raman spectroscopy. Am Mineral 91:459–462

Schmidt MW, Poli S (1998) Experimentally based water budgets for dehydrating slabs and consequences for arc magma generation. Earth Planet Sci Lett 163:361–379

Schwartz S, Allemand P, Guillot S (2001) Numerical model of the effect of serpentinites on the exhumation of eclogitic rocks: insights from the Monviso ophiolitic massif (Western Alps). Tectonophysics 342:193–206

Ulmer P, Trommsdorff V (1995) Serpentine stability to mantle depths and subduction-related magmatism. Science 268:858–861

Viti C, Mellini M (1997) Contrasting chemical compositions in associated lizardite and chrysotile in veins from Elba, Italy. Eur J Mineral 9:585–596

Wicks FJ, O'Hanley DS (1988) Serpentine minerals: structures and petrology. In: Bailey SW (ed) Hydrous phyllosilicates (exclusive of Micas). Mineralogical Society of America, Washington, pp 91–167

Wunder B, Schreyer W (1997) Antigorite: high-pressure stability in the system $MgO–SiO_2–H_2O$(MSH). Lithos 41:213–227